Cardiac ^{123}I-MIBG planar heart to mediastinum ratios depend on patient size; phantom studies suggest SPECT-CT could improve quantification

Gemma Roberts[1,2], Jim J. Lloyd[1,2], George S. Petrides[2], John T. O'Brien[3], Alan J. Thomas[1]

1: Institute of Neuroscience, Newcastle University, Biomedical Research Building, Campus for Ageing and Vitality, Westgate Road, Newcastle upon Tyne, UK. NE4 6BE

2: Nuclear Medicine Department, Leazes Wing, Royal Victoria Infirmary, Richardson Road, Newcastle upon Tyne, UK. NE1 4LP

3: Department of Psychiatry, University of Cambridge, Box 189, Level E4 Cambridge Biomedical Campus, Cambridge, CB2 0SP

Corresponding author:

Gemma Roberts

Institute of Neuroscience, Newcastle University, Biomedical Research Building, Campus for Ageing and Vitality, Westgate Road, Newcastle upon Tyne, UK. NE4 6BE

gemma.roberts@newcastle.ac.uk

ORCID ID: 0000-0002-6445-4023

Abstract

Introduction:

Planar ^{123}I-MIBG (meta-iodobenzylguanidine) cardiac imaging is listed as an indicative biomarker in the 2017 international consensus criteria for the diagnosis of dementia with Lewy bodies. There has been very little research into the relationship between apparent cardiac uptake and patient size, or in the possible advantage of attenuation and scatter corrected SPECT-CT compared to planar imaging. We aimed to evaluate this in both a chest phantom and in older adults with normal cognition.

Materials and Methods:

An anthropomorphic chest phantom was filled with ^{123}I solution using activities typical of healthy subjects. The phantom was scanned on a Siemens Intevo gamma camera with MELP collimators using both planar and SPECT-CT techniques. Further scans were acquired with a PMMA chest plate added, then water filled plastic breasts. The SPECT-CT images were reconstructed using a resolution recovery OSEM method with and without attenuation and scatter correction (ACSC) applied.

Twenty-nine adults over 60 years of age (mean 75.2 ± 8.3 years) underwent planar cardiac MIBG imaging, followed by SPECT-CT. SPECT images were reconstructed as above. Heart-to-mediastinum ratios (HMRs) were calculated for planar and SPECT images.

Results:

Phantom planar HMR decreased by 20% with the PMMA chest plate added; 39% with plate and breasts. ACSC SPECT cardiac counts showed less dependence on phantom size than SPECT without ACSC (3% vs 37%). The body mass indices (BMI) of the older adults ranged from 22 to 38. There was a significant linear relationship between planar HMR and BMI (R^2=0.44, p<0.01), but not for ACSC SPECT. However, there was no significant difference between the slopes for planar and ACSC SPECT (p=0.11).

Conclusion:

Planar cardiac ^{123}I-MIBG HMR results are correlated with BMI. Phantom results suggest that ACSC SPECT can correct for patient size. A large patient population or clinical database would be required to demonstrate a clinical effect.

Introduction

Dementia with Lewy bodies (DLB) is the second most common form of neurodegenerative dementia after Alzheimer's disease, accounting for 5-10% of cases [1, 2]. Accurate diagnosis is important for clinical management, prognosis, and carer wellbeing [3-5], but initial misdiagnosis outside the specialist setting is common [2, 6, 7]. Cardiac MIBG sympathetic innervation imaging is an established technique for the differential diagnosis of DLB from other dementias, which do not cause sympathetic denervation and thus have normal scan appearances [8-10]. The technique has been used in Japan for the diagnosis of Lewy body disease for over a decade and was recently included as an indicative biomarker in the fourth DLB consensus criteria, alongside ^{123}I-FP-CIT SPECT [6]. Cardiac MIBG scintigraphy is also used for the estimation of risk of sudden cardiac death in heart failure patients and predicting those who could benefit from an implantable cardiac defibrillator (ICD) [11, 12] and this is currently the principal application in Europe and the US [13].

Several authors have commented on the need to standardise cardiac MIBG image acquisition and processing parameters in order for cardiac uptake thresholds to be applicable between centres, e.g. [14-19]. A method to correct for differences in image acquisition parameters between centres (predominantly caused by different gamma camera and collimator models) has been developed by Nakajima *et al.* [20] was used in the multicentre study mentioned above [21, 22]. However, technical factors such as variation in the amount of attenuation and scatter due to patient size, cannot be taken into account with this method. There have been few publications commenting on whether patient factors may have a significant impact on diagnostic value of planar cardiac MIBG scintigraphy, and to our knowledge none that have explored whether SPECT with CT attenuation and scatter correction (CTACSC) would be of benefit. Although several groups investigating the diagnostic accuracy of cardiac ^{123}I-MIBG for the diagnosis of Lewy body disease have acquired SPECT data alongside planar, often it is only the planar scans that have been used for analysis with the SPECT results not reported [23-27], suggesting the added value of SPECT is unclear. In 2016 Odagiri *et al.* reported that the accuracies of planar and SPECT-CT ^{123}I-MIBG cardiac scintigraphy were similar, but did not appear to use the CT data for SPECT image corrections, only for localising the heart [28]. In their 2015 multicentre study, Yoshita *et al.* used SPECT for visual analysis but not for quantification of cardiac uptake [21].

Obesity has been linked to decreased apparent cardiac MIBG uptake by two previous studies [29, 30], and is thought to be due to increased attenuation and scatter in larger individuals, rather than to true differences in cardiac uptake. The largest study of healthy controls recruited to a cardiac MIBG research study (n=94) was that of Jacobsen et al. [31] carried out as part of the ADMIRE heart failure study [11]. The controls were aged between 29 to 82 years (mean 58.5 ± 10.6 years, with a wide BMI

range of 20.4 to 44.3 kg/m^2 (mean 28.7 ± 5.1). The study reported a "modest" decrease in HMR with BMI, however this was a study into ageing and the incidental finding of a relationship between BMI and HMR was not discussed in detail. Pellegrino *et al.* reported lower HMRs in patients with BMI>30 (n=10) compared to those with BMI<30 (n=35) [30]. This was in heart failure patients and the results have not yet been replicated in healthy controls but do suggest patient size may affect apparent cardiac MIBG uptake.

In this study we aimed to establish the degree to which planar cardiac I-123-MIBG scintigraphy is affected by patient size and whether SPECT with CTACSC can correct for this. We investigated this using an anthropomorphic chest phantom configured with different amounts of attenuation and a cohort of older adults with normal cognition with BMI between 22 and 38 kg/m^2.

Materials and methods

Inclusion criteria for older adults

Twenty-nine volunteers aged between 62 and 94 years (mean 75.2 ± 8.3 years) were recruited as part of an ongoing Newcastle University study into cardiac MIBG in a representative UK population of older adults. They underwent a detailed neurological and cognitive examination by a research physician with a detailed medical history taken. All volunteers had normal cognition, no evidence of parkinsonism and normal MRI brain scans. We did not recruit anyone with Class II or worse heart failure according to the New York Heart Association classification, who had experienced a myocardial infarction in the previous year or were taking tramadol. As we aimed to recruit a representative sample of older people, we did not exclude those with diabetes or other risk factors for cardiac disease such as smoking or raised blood pressure.

Image acquisition

The volunteers were administered 111 MBq I-123-MIBG via slow intravenous injection. Potassium iodate tablets (170mg) were given before and after injection to minimise uptake of free iodine by the thyroid. Ten minute anterior planar images were acquired at 4 hours (± 30 minutes) after injection. SPECT-CT imaging was carried out immediately after the delayed planar image with the subject in the supine position with arms raised if possible. Only ten of the volunteers were able to be scanned with arms raised, the others kept their arms by their sides. All images were acquired on a dual headed Siemens Symbia Intevo hybrid SPECT-CT gamma camera (Siemens Healthcare, Munich, Germany) using medium energy low penetration (MELP) collimators. For planar imaging the energy window was 159 keV $\pm$ 10%, matrix size was 128 x 128 and no zoom was applied, resulting in a pixel size of 4.8 mm.

SPECT images were acquired over 360 degrees in H mode (detectors oriented parallel to each other) to obtain 120 projections of 20 seconds using a non-circular autocontoured orbit. The energy window was 159 keV ± 7.5%, matrix size 64 x 64 and zoom factor 1.64. Following SPECT imaging, a low dose CT scan (130 kV with a quality reference mAs of 13) was acquired for attenuation and scatter correction.

Image reconstruction

All images were processed on a Hermes workstation (Hermes Medical Ltd, Stockholm Sweden), to obtain results generalisable to different gamma camera models. SPECT images were processed in Hermes Hybrid Recon Cardiology v1.1.2 using OSEM iterative reconstruction with 15 iterations and 3 subsets, with a Butterworth filter of 0.90 cm applied. Resolution recovery collimator modelling for the MELP collimator was applied, with parameters set for the Siemens Intevo gamma camera as provided by Hermes: hole diameter 0.294 cm; hole length 4.06 cm; detector intrinsic resolution at 140 keV 0.38 cm ; radius of rotation off-set 4.76 cm. Two sets of images were reconstructed, both using resolution recovery: non-corrected (NC) and CT corrected for attenuation and scatter (ACSC). The voxel size was 6.6 mm. The scatter correction model is based on a Monte Carlo simulation of scatter within the patient [32, 33]. Full collimator and detector response modelling [34] is not included in this model.

Phantom image acquisition

Images were acquired with the RSD torso phantom (Radiology Support Devices Ltd, Long Beach, CA, USA), with fillable heart, lung, liver and background compartments (Figure 1). The original heart insert supplied with the phantom did not give realistic-looking cardiac MIBG images so was substituted with a simple left ventricle insert manufactured in-house with fillable myocardial wall and cavity compartments. The phantom was filled and scanned with I-123, using activity concentrations designed to mimic patient studies. The activities used are given in Table 1. The left ventricle insert was imaged alone on the scanner bed without any additional attenuation followed by three filled phantom scans with increasing amounts of attenuation: torso phantom, torso phantom with solid PMMA chest extension plate and torso phantom with chest plate and breasts (plastic shells filled with water) – see Figure 1.

The scan parameters were the same as those used for clinical research studies at our centre: MELP collimators, auto-contouring, 1.64 zoom, 64 x64 matrix size. As with clinical scans, CT scans allow for both attenuation and scatter corrected and non-corrected images to be reconstructed..

Images were reconstructed using the clinical parameters given above.

Figure 1: Anthropomorphic torso phantom (centre), with in-house replacement LV insert (left) and additional PMMA chest plate and water filled breasts (right)

Table 1: activity concentrations used in the anthropomorphic torso phantom, selected to give count densities similar to healthy control images.

	Activity (MBq)	Activity concentration (kBq / ml)	Concentration relative to background
LV dose (diluted into 200 ml, actual volume ~160 ml)	27.7	138.7	22
Background (approx. 8200 ml)	52.6	6.4	1
Liver (1000 ml)	78.6	78.6	12.2
Lungs (diluted in 1000 ml before filling)	50.1	50.1	7.8

Image analysis for cardiac uptake

The images of the torso phantom and the images of the older adult volunteers were analysed in the same way. Anterior planar images were analysed to obtain the heart to mediastinum ratio (HMR) using a 6 cm circular ROI placed over the left ventricle and 4 x 3 cm rectangular ROI between the lungs in the mediastinum, see [35]. The phantom was not moved from the scanner couch between acquisitions, allowing the same regions to be used for all three attenuation configurations.

The SPECT coronal slices were summed over all 64 slices to give images analogous to planar images. We obtained HMRs on these summed images in the same way as for the planar and we term these "coronal SPECT HMRs". The same regions of interest were used for planar and summed coronal SPECT

HMRs, with no adjustment between the non-corrected and ACSC SPECT (see Figure 2 for example). This enables a direct assessment of the effects of attenuation and scatter correction to be made.
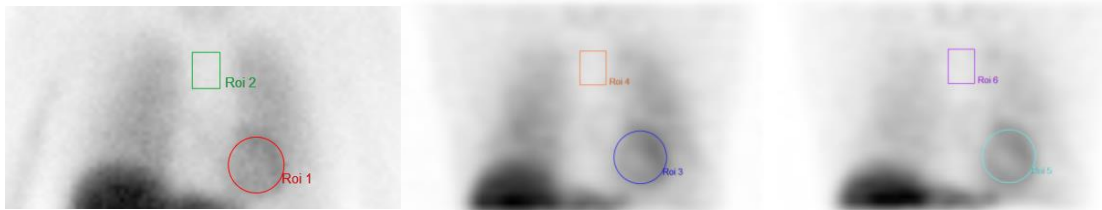

Figure 2: Planar image (left) with corresponding summed coronal SPECT slice images without CT ACSC (middle) and with corrections (right). Note the relative reduction in lung uptake and increased heart contrast on the ACSC image.

Volumetric HMRs on clinical and phantom SPECT images were calculated using 6cm diameter spherical VOIs placed over the left ventricle and cuboid VOIs over the mediastinum (Figure 3). The placement of VOIs was not modified between the ACSC and non-corrected datasets.
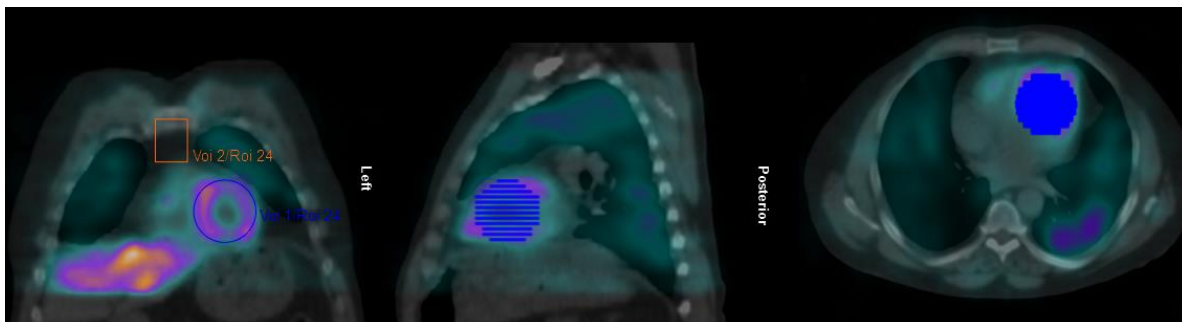
Figure 3: Example control SPECT-CT images showing coronal, sagittal and transverse slices centred on the left ventricle, with spherical cardiac VOI and rectangular mediastinal VOI shown.

Planar and SPECT HMR data for the controls were plotted against BMI and the slopes and standard errors calculated using linear regression. The standard errors of the slopes were used to calculate t-statistics to determine whether each relationship between HMR and BMI (for planar or SPECT) was significant at the $\alpha = 0.05$ level. To compare slopes, normalisation was necessary since average HMRs are much higher for SPECT than planar due to increased contrast. The SPECT slopes and the standard errors were scaled to be consistent with planar data by multiplying by the ratio between the mean planar HMR and HMR in question. The differences between the normalised slopes and their combined standard errors were used to determine whether corrections for attenuation and scatter had a significant impact on reducing the dependence of HMR on BMI.

Results

Torso phantom

The appearance of the phantom on planar and non-corrected SPECT images was significantly affected by additional attenuation, whereas this was not the case with the attenuation and scatter corrected SPECT images (Figure 4). The HMR on planar imaging was reduced by 20% with the additional PMMA chest plate added and by 40% with the plate and water filled breasts added (Figure 4 and Figure 5). On the summed coronal SPECT images without CT ACSC this improved to 11% and 21% respectively. The summed coronal ACSC SPECT images showed an increase in HMR with additional attenuation, due to lower mediastinum counts – the appearance of the images was reasonably preserved.

Compared to baseline, the volumetric HMR with the additional chest plate and breasts decreased from 8.8 to 7.6 (13%) on non-corrected SPECT but increased from 9.5 to 10.3 (8%) on ACSC (Figure 5), again due to a greater reduction in counts in the mediastinum VOI.

The decay corrected SPECT cardiac count data (Figure 6), show a much lower drop with additional attenuation on the ACSC images than the non-corrected SPECT images (3% vs 37%).

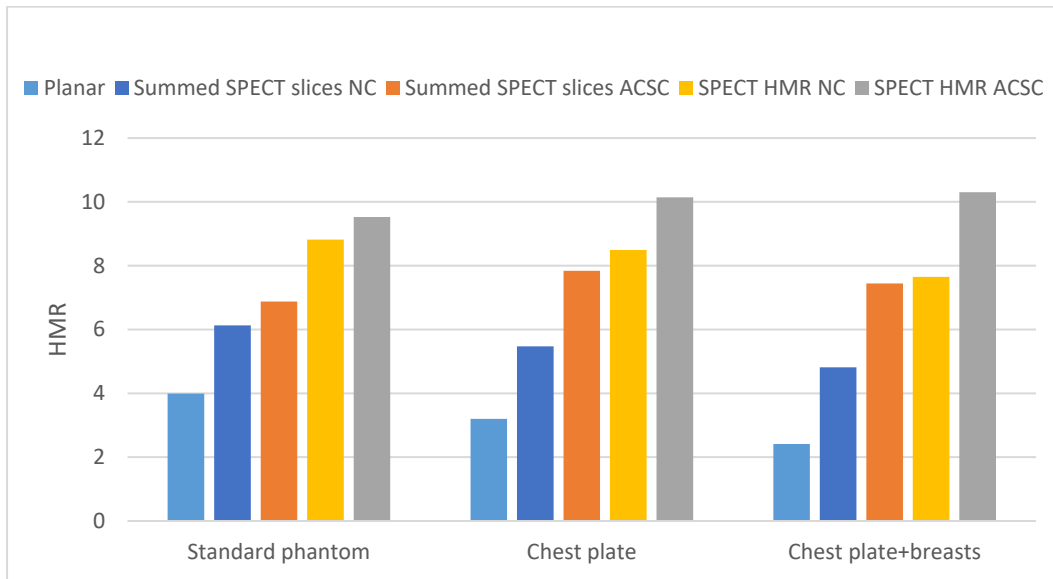|	Standard torso phantom	With chest plate attenuation	With chest plate and breast attenuation
Standard planar imaging			
	HMR = 3.99	HMR = 3.20 (-20%)	HMR 2.41 (-40%)
Summed coronal NC SPECT slices			
	HMR = 6.13	HMR = 5.47 (-11%)	HMR = 4.82 (-21%)
Summed coronal ACSC SPECT slices			
	HMR = 6.87	HMR = 7.84 (+14%)	HMR = 7.44 (+8%)

Figure 5: Phantom heart to mediastinum ratios for the three size configurations, calculated from planar images, summed ACSC and non-corrected (NC) coronal SPECT images and volumetric HMRs from ACSC and NC SPECT. Both the planar and non-corrected SPECT HMRs decrease with additional attenuating material.
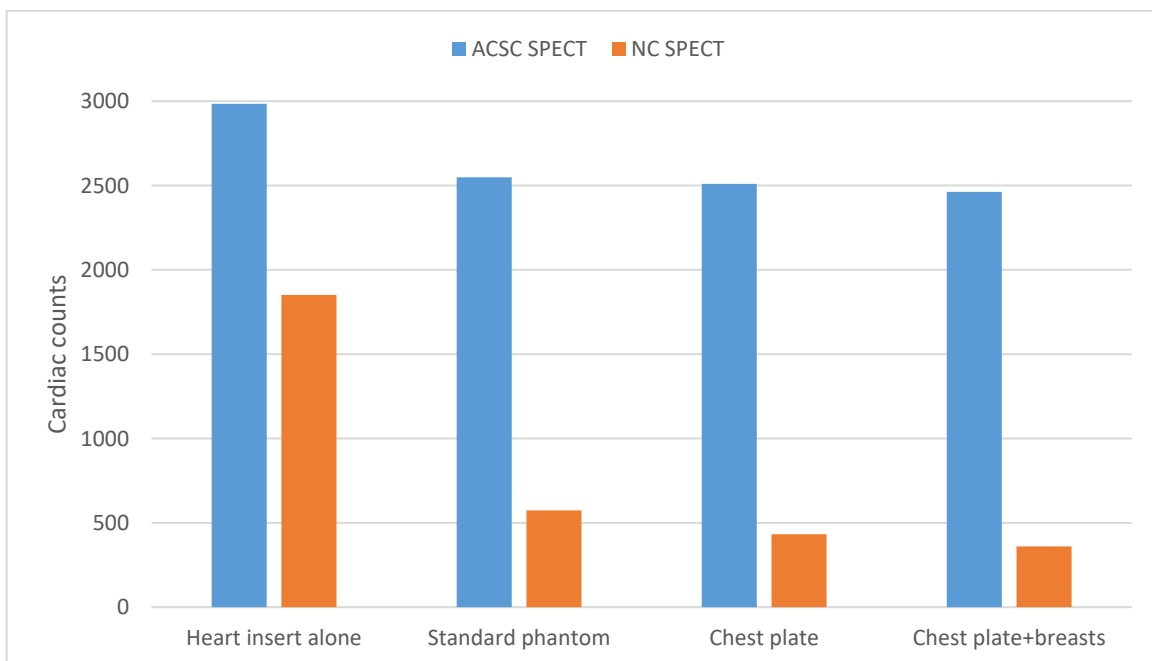

Figure 6: Counts in cardiac volume of interest with ACSC and non-corrected SPECT for the heart insert scanned alone and with increasing attenuation within the torso phantom. The decrease in counts when the insert is scanned within the phantom is much less with ACSC applied, as is the difference between the standard phantom configuration and the largest size.

Clinical results

On planar imaging a negative linear correlation between HMR and BMI is seen (Figure 7), with a slope that is significantly different from zero (p <0.01), resulting in a 32% drop in HMR on average between BMI of 20 and 35 (

Table 2). In comparison, the drop in HMR over this BMI range with attenuation and scatter corrected SPECT was 14% on average for the summed coronal slice method and 16% for the volumetric SPECT method (with 6cm diameter spherical VOI). However, comparison between normalised slope values, via a t-statistic calculated from the standard errors of the slopes (Table 3) shows no significant difference between planar and either summed coronal ACSC SPECT (p =0.11) or volumetric ACSC SPECT (p=0.36).

Error! Reference source not found. shows the plots of HMR or cardiac counts against BMI for the summed coronal SPECT images and SPECT volumetric HMR. These are displayed with the non-corrected data on the left and the ACSC data on the right for each method. The linear fits, and p values for slopes being different from zero for planar and SPECT imaging are given in

Table 2. The p-values in show that with the summed non-corrected SPECT coronal slices, there is a significant drop in HMR with BMI but with attenuation and scatter correction this is not statistically significant. However, when comparing the slopes for non-corrected and ACSC coronal HMR data directly (

Table 2) there is no evidence of a statistically significant difference. SPECT volumetric HMR (spherical VOI) data show no significant relationship with BMI either with or without ACSC, and have the highest normalised standard errors, possibly due to greater uncertainty in cardiac and mediastinum volume of interest placement compared to the other 2D methods. The coefficients of variation of the HMR data (independent of any relationship with BMI) are also higher for the volumetric SPECT data than for the planar or summed coronal HMRs (
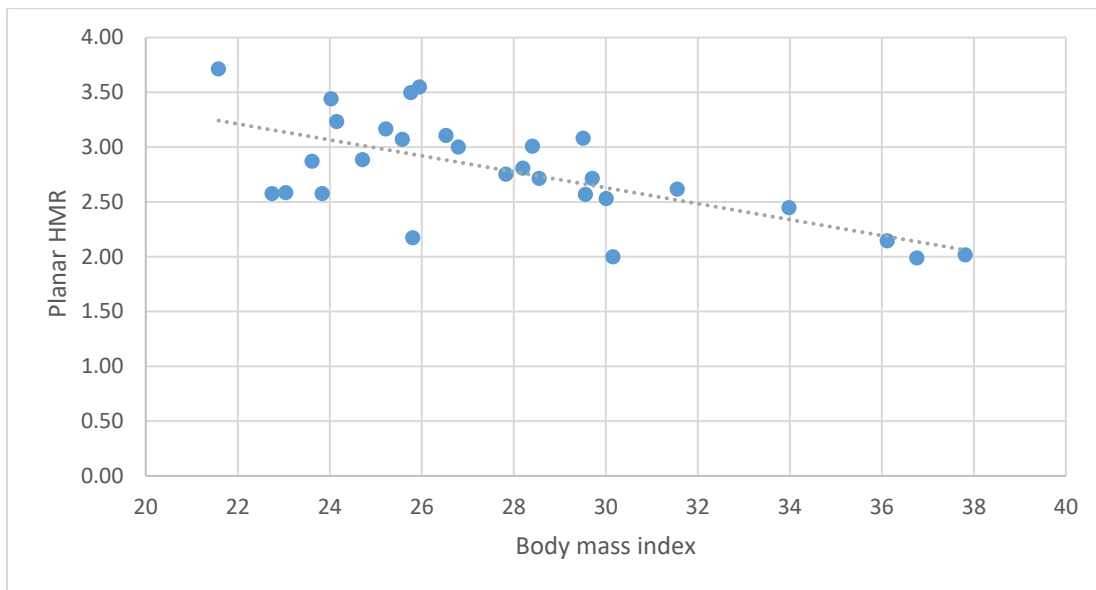
Table 2).

Figure 7: planar HMR plotted against BMI for the 29 older adults, with linear fit.

Table 2: Linear regression between HMR and BMI for planar data and SPECT with and without attenuation and scatter correction.

Quantitative measurement	Planar HMR	Summed SPECT coronal slices HMR		Volumetric SPECT HMR	
CT ACSC?	n/a	Yes	No	Yes	No
Coefficient of variation	17%	14%	13%	25%	28%
Linear fit to BMI	-0.067*BMI + 4.61	-0.039*BMI + 4.76	-0.053*BMI + 4.74	-0.117*BMI + 12.84	-0.125*BMI + 12.42
R^2	0.44	0.11	0.28	0.05	0.05
Normalised slope	n/a	-0.028	-0.037	-0.034	-0.039
SE of slope	0.017	0.023	0.017	0.104	0.11
Normalised SE	n/a	0.017	0.015	0.03	0.034
p-value for non-zero slope	<0.01	0.09	<0.01	0.27	0.27
Predicted drop in value between BMI 20 and 35	3.36 to 2.27 (-32%)	3.95 to 3.39 (-14%)	3.69 to 2.90 (-21%)	10.50 to 8.74 (-16%)	9.93 to 8.06 (-19%)

Table 3: Comparison between normalised slopes for planar and SPECT HMR with BMI, and for attenuation and scatter corrected SPECT data vs no corrections.

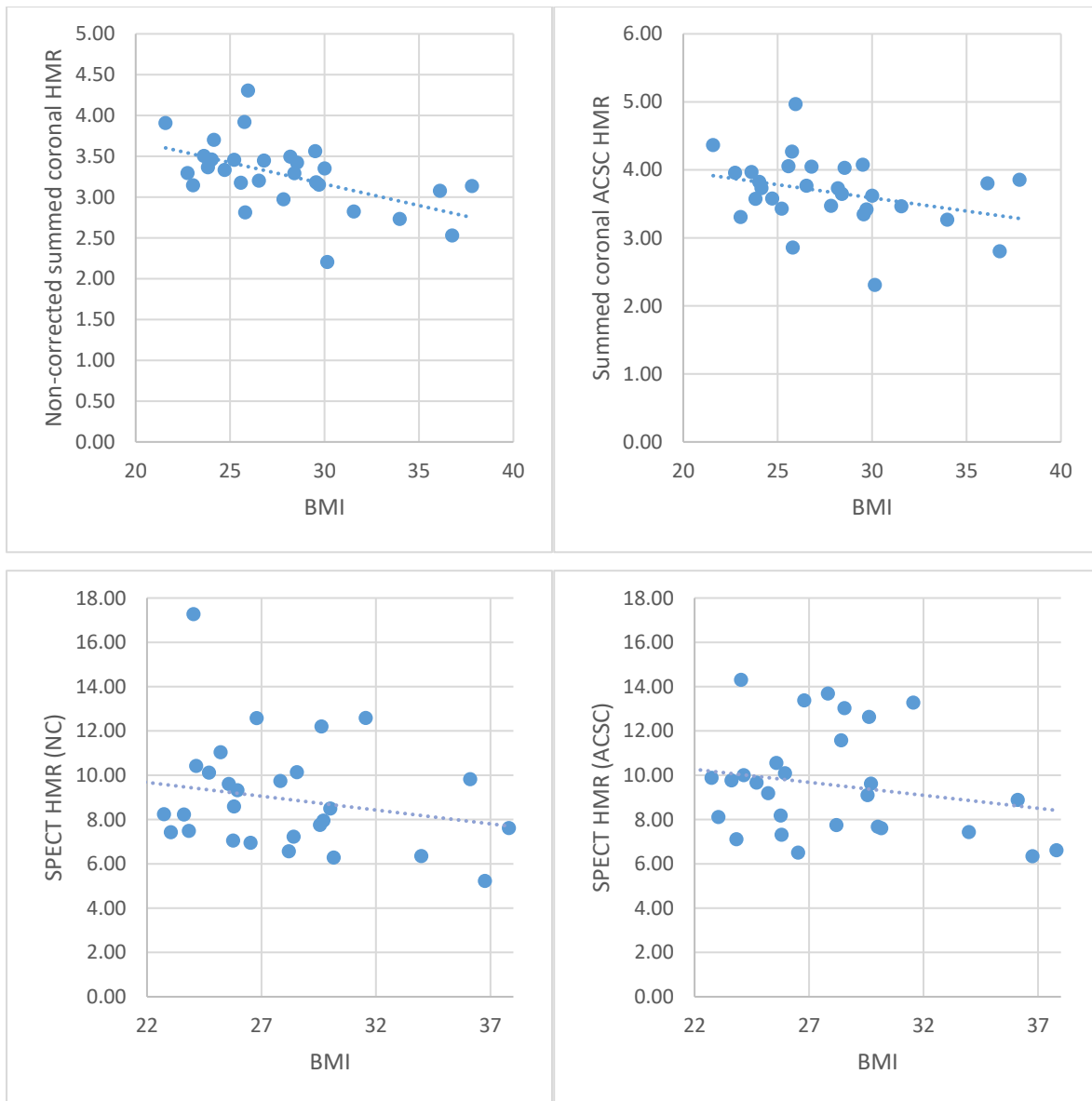| Comparison	Difference in normalised slopes	Combined normalised standard error	T-statistic	P-value
Planar HMR vs ACSC summed coronal HMR	0.038	0.022	1.60	0.11
Planar HMR vs ACSC volumetric SPECT HMR	0.032	0.035	0.932	0.36
Summed coronal: ACSC vs no corrections	0.008	0.022	0.380	0.71
Volumetric SPECT: ACSC vs no corrections	0.005	0.046	0.104	0.92

Figure 8: Summed coronal HMR with and without ACSC (top), SPECT volumetric HMR with and without ACSC (bottom).

Discussion

A strength of our study is the inclusion of both phantom and clinical data. The phantom data was acquired under controlled conditions allowing us to investigate the impact of increasing phantom size alone with no other sources of variation. The clinical data applies image reconstruction in more realistic conditions to determine whether the effect holds in practice.

The visual appearance of the torso phantom reconstructed with the summed ACSC SPECT images was greatly improved compared to the standard planar images and the non-corrected summed SPECT

images; this is particularly apparent on the third configuration with both the PMMA chest plate and the water filled breast inserts added. The counts within the left ventricle insert showed a much greater reduction with increasing scatter and attenuation on the non- corrected images compared to those reconstructed with ACSC. Given that this was an anthropomorphic phantom with realistic dimensions and activity concentrations, the results can be assumed to hold in individual patients.

However, when examining our cohort of 29 older adults with normal cognition, the benefit of ACSC SPECT is not as apparent. Although on average, the relationship between BMI and cardiac uptake was less obvious with SPECT imaging than planar, there was no evidence that this was statistically significant. It is clear that there is a significant relationship between planar HMR and body mass index, so on average we would expect to see lower HMRs in larger people. However given the substantial variation between subjects (an R^2 value of 0.44 suggests that less than half the variation is related to BMI), it would not be practical to apply a linear correction to the HMR results based on BMI. This variation seems to be even greater with SPECT volumetric HMRs and there is furthermore no statistically significant negative slope between SPECT HMR and BMI, which we would expect for data without attenuation and scatter correction if this is the cause of the drop seen in planar imaging. The summed coronal slices do show a drop on the non-corrected images, suggesting that the summation of the SPECT slices reduces noise in the data. We recognise that BMI is more complex than the increases in size applied to our phantom study and there is likely to be substantial variation in the gamma ray interactions of two people of the same BMI. The size of the left ventricle may also affect the activity concentration. In addition, the inactive background material used in the phantom is not fully representative of the activity distribution within patients.

Variation in uptake between individuals may not be the only explanation for our findings. The ACSC summed coronal SPECT images do not appear noisier than the planar images but do suggest a drop in HMR with increasing BMI, albeit not statistically significant. A possible explanation is errors in the CT ACSC that are not seen in the phantom scans. Motion between SPECT and CT is a possibility, either due to volunteers moving slightly or internal mis-registration due to free breathing (e.g. diaphragm) or lack of cardiac gating. The images were examined for mis-registration during reconstruction, but this will not detect subtle shifts.

A further limitation is the truncation of reconstructed SPECT data in some cases, due to the finite field of view. The majority of the older adults (19/29) were not able to tolerate being scanned with their arms raised, which is the standard protocol, so the arms were outside the SPECT field of view and not taken into account during reconstruction (Figure 9). The CT field of view is slightly wider, but the CT data outside the SPECT field is not used for reconstruction. In some cases there was further truncation

due to body habitus for the largest subjects. This means that scatter and attenuation correction for larger people may be inadequate, and could explain why there appears to be a residual drop in ACSC SPECT HMR with increasing BMI (Figure 10). However, we cannot exclude the possibility that larger people may on average be more likely to have true reductions in cardiac uptake, for example due to underlying coronary artery disease, for which obesity is a risk factor.
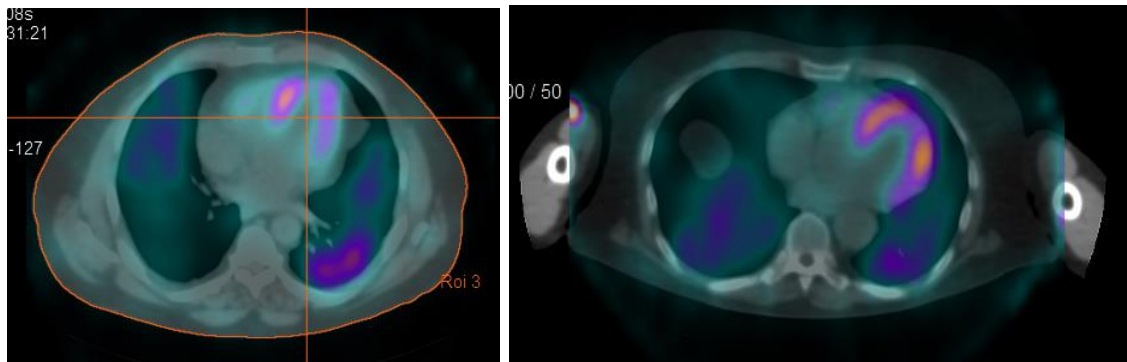

Figure 9: The image on the left is of a volunteer scanned with arms raised, with the whole body within the SPECT and CT fields of view. The image on the right is an example of a larger person scanned with arms by their side. The arms are outside the SPECT field of view so have not been taken into account.
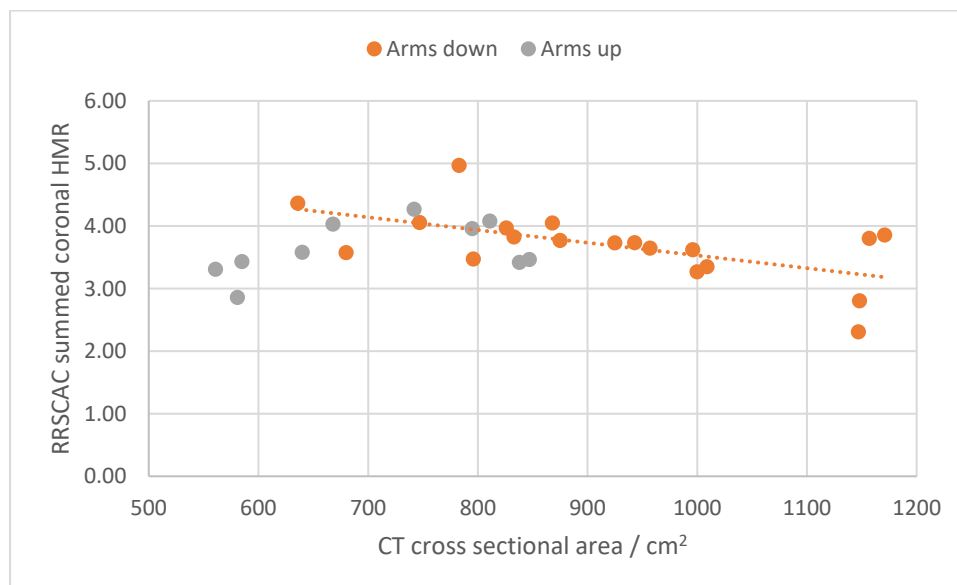

Figure 10: Attenuation and scatter corrected HMR for the volunteers plotted against cross sectional size on CT. For those scanned with arms down there appears to be drop in HMR with size, suggesting inadequate ACSC due to data truncation.

Conclusion

In an anthropomorphic torso phantom, increasing the size reduces cardiac uptake on planar images and on non-corrected SPECT images, but with attenuation and scatter correction applied the reduction

is no longer apparent. Clinical planar cardiac ^{123}I-MIBG images show a significant inverse relationship between cardiac uptake ratios and subject BMI. SPECT images with attenuation and scatter correction applied show no statistically significant drop in cardiac uptake with BMI, but there is considerable inter-subject variation and no statistically significant difference between the slopes of HMR against BMI for non-corrected and ACSC SPECT. It may be possible to reduce variation in future studies by using a SPECT-CT protocol that is more acceptable to older patients. This work suggests that ACSC SPECT does have the potential to improve cardiac ^{123}I-MIBG quantification, particularly in borderline planar cases but much larger studies would be needed to demonstrate this.

Participant Consent and Ethical Approval

All procedures performed in studies involving human participants were in accordance with the ethical standards of the Newcastle University and Newcastle upon Tyne NHS Foundation Trust research committee and with the 1964 Helsinki declaration and its later amendments or comparable ethical standards. Informed consent was obtained from all individual participants included in the study.

Acknowledgements

References

1. Vann Jones, S.A. and J.T. O'Brien, *The prevalence and incidence of dementia with Lewy bodies: a systematic review of population and clinical studies.* Psychol Med, 2014. **44**(4): p. 673-83.
2. Kane, J.P.M., et al., *Clinical prevalence of Lewy body dementia.* Alzheimers Res Ther, 2018. **10**(1): p. 19.
3. Hanyu, H., et al., *Differences in clinical course between dementia with Lewy bodies and Alzheimer's disease.* Eur J Neurol, 2009. **16**(2): p. 212-7.
4. Lee, D.R., et al., *Examining carer stress in dementia: the role of subtype diagnosis and neuropsychiatric symptoms.* Int J Geriatr Psychiatry, 2013. **28**(2): p. 135-41.
5. Galvin, J.E., et al., *Lewy body dementia: the caregiver experience of clinical care.* Parkinsonism Relat Disord, 2010. **16**(6): p. 388-92.
6. McKeith, I.G., et al., *Diagnosis and management of dementia with Lewy bodies: Fourth consensus report of the DLB Consortium.* Neurology, 2017. **89**(1): p. 88-100.
7. Donaghy, P.C. and I.G. McKeith, *The clinical characteristics of dementia with Lewy bodies and a consideration of prodromal diagnosis.* Alzheimers Res Ther, 2014. **6**(4): p. 46.
8. Chung, E.J. and S.J. Kim, *(123)I-Metaiodobenzylguanidine Myocardial Scintigraphy in Lewy Body-Related Disorders: A Literature Review.* J Mov Disord, 2015. **8**(2): p. 55-66.
9. Orimo, S., et al., *(123)I-meta-iodobenzylguanidine (MIBG) cardiac scintigraphy in alpha-synucleinopathies.* Ageing Res Rev, 2016. **30**: p. 122-33.
10. Sonni, I., et al., *Clinical validity of presynaptic dopaminergic imaging with (123)I-ioflupane and noradrenergic imaging with (123)I-MIBG in the differential diagnosis between Alzheimer's disease and dementia with Lewy bodies in the context of a structured 5-phase development framework.* Neurobiol Aging, 2017. **52**: p. 228-242.
11. Jacobson, A.F., et al., *Myocardial iodine-123 meta-iodobenzylguanidine imaging and cardiac events in heart failure. Results of the prospective ADMIRE-HF (AdreView Myocardial Imaging for Risk Evaluation in Heart Failure) study.* J Am Coll Cardiol, 2010. **55**(20): p. 2212-21.
12. Verberne, H.J., et al., *Prognostic value of myocardial 123I-metaiodobenzylguanidine (MIBG) parameters in patients with heart failure: a systematic review.* Eur Heart J, 2008. **29**(9): p. 1147-59.
13. Travin, M.I., et al., *How do we establish cardiac sympathetic nervous system imaging with (123)I-mIBG in clinical practice? Perspectives and lessons from Japan and the US.* J Nucl Cardiol, 2018.
14. Nakajima, K., et al., *Standardization of 123I-meta-iodobenzylguanidine myocardial sympathetic activity imaging: phantom calibration and clinical applications.* Clin Transl Imaging, 2017. **5**(3): p. 255-263.
15. Verberne HJ, et al., *Vascular time-activity variation in patients undergoing ^{123}I-MIBG myocardial scintigraphy: implications for quantification of cardiac and mediastinal uptake.* Eur J Nucl Med Mol Imaging, 2011. **38**(6): p. 7.
16. Verschure DO, et al., *^{123}I-MIBG heart-to-mediastinum ratio is influenced by high-energy photon penetration of collimator septa from liver and lung activity.* Nucl Med Commun, 2015. **36**(3): p. 7.
17. Verschure, D.O., et al., *A European myocardial 123I-mIBG cross-calibration phantom study.* J Nucl Cardiol, 2017.

18.   Slomka, P., et al., *Quantification of I-123-meta-iodobenzylguanidine Heart-to-Mediastinum Ratios: Not So Simple After All.* J Nucl Cardiol, 2014. **21**: p. 979-983.

19.   Klene, C., et al., *Influence of ROI definition on the heart-to-mediastinum ratio in planar 123I-MIBG imaging.* J Nucl Cardiol, 2016.

20.   Nakajima, K., et al., *Standardization of metaiodobenzylguanidine heart to mediastinum ratio using a calibration phantom: effects of correction on normal databases and a multicentre study.* Eur J Nucl Med Mol Imaging, 2012. **39**(1): p. 113-9.

21.   Yoshita, M., et al., *Diagnostic accuracy of 123I-meta-iodobenzylguanidine myocardial scintigraphy in dementia with Lewy bodies: a multicenter study.* PLoS One, 2015. **10**(3): p. e0120540.

22.   Komatsu, J., et al., *(123)I-MIBG myocardial scintigraphy for the diagnosis of DLB: a multicentre 3-year follow-up study.* J Neurol Neurosurg Psychiatry, 2018.

23.   Hanyu, H., et al., *The role of 123I-metaiodobenzylguanidine myocardial scintigraphy in the diagnosis of Lewy body disease in patients with dementia in a memory clinic.* Dement Geriatr Cogn Disord, 2006. **22**(5-6): p. 379-84.

24.   Inui, Y., et al., *Comparison of (123)I-MIBG myocardial scintigraphy, brain perfusion SPECT, and voxel-based MRI morphometry for distinguishing between dementia with Lewy bodies and Alzheimer's disease.* Ann Nucl Med, 2014. **28**(8): p. 796-804.

25.   Oide, T., et al., *Usefulness of [123I]metaiodobenzylguanidine ([123I]MIBG) myocardial scintigraphy in differentiating between Alzheimer's disease and dementia with Lewy bodies.* Intern Med, 2003. **42**(8): p. 686-90.

26.   Wada-Isoe, K., et al., *Diagnostic markers for diagnosing dementia with Lewy bodies: CSF and MIBG cardiac scintigraphy study.* J Neurol Sci, 2007. **260**(1-2): p. 33-7.

27.   Watanabe, H., et al., *Cardiac (123)I-meta-iodobenzylguanidine (MIBG) uptake in dementia with Lewy bodies: comparison with Alzheimer's disease.* J Neurol Neurosurg Psychiatry, 2001. **70**(6): p. 781-3.

28.   Odagiri, H., et al., *On the Utility of MIBG SPECT/CT in Evaluating Cardiac Sympathetic Dysfunction in Lewy Body Diseases.* PLoS One, 2016. **11**(4): p. e0152746.

29.   Jacobson AF, et al., *Impact of age on myocardial uptake of 123I-mIBG in older adult subjects without coronary heart disease. .* J Nucl Cardiol, 2013. **20**: p. 9.

30.   Pellegrino, T., et al., *Impact of obesity and acquisition protocol on (123)I-metaiodobenzylguanidine indexes of cardiac sympathetic innervation.* Quant Imaging Med Surg, 2015. **5**(6): p. 822-8.

31.   Jacobson, A.F., et al., *Impact of age on myocardial uptake of (1)(2)(3)I-mIBG in older adult subjects without coronary heart disease.* J Nucl Cardiol, 2013. **20**(3): p. 406-14.

32.   Sohlberg, A., H. Watabe, and H. Iida, *Acceleration of Monte Carlo-based scatter compensation for cardiac SPECT.* Phys Med Biol, 2008. **53**(14): p. N277-85.

33.   Kangasmaa, T., et al., *Half-time myocardial perfusion SPECT imaging with attenuation and Monte Carlo-based scatter correction.* European Journal of Nuclear Medicine and Molecular Imaging, 2011. **38**: p. S204-S204.

34.   Sohlberg, A.O. and M.T. Kajaste, *Fast Monte Carlo-simulator with full collimator and detector response modelling for SPECT.* Annals of Nuclear Medicine, 2012. **26**(1): p. 92-98.

35.   Roberts, G., et al., *A comparison of visual and semiquantitative analysis methods for planar cardiac 123I-MIBG scintigraphy in dementia with Lewy bodies.* Nucl Med Commun, 2019.